Immunologically distinct responses occur in the CNS of COVID-19 patients

Eric Song[1,*], Ryan D Chow[2,3], Ruoyi Jiang[1], Colin R. Zamecnik[4,5], Rita P Loudermilk[4,5], Yile Dai[1], Feimei Liu[1], Bertie Geng[6,7], Jennifer Chiarella[8], Benjamin Israelow[1,6], Arnau Casanovas-Massana[9], Albert I Ko[9], Aaron Ring[1], Steven H. Kleinstein[1,10,11], Serena Spudich[8], Michael R Wilson[4,5], Akiko Iwasaki[1,12,13], Shelli F. Farhadian[6,8,*]

[1] Department of Immunobiology, Yale School of Medicine, New Haven, CT, USA

[2] Department of Genetics, Yale School of Medicine, New Haven, CT, USA

[3] Systems Biology Institute, Yale School of Medicine, New Haven, CT, USA

[4] Weill Institute for Neurosciences, University of California, San Francisco, CA, USA

[5] Department of Neurology, University of California, San Francisco, CA, USA

[6] Department of Internal Medicine, Section of Infectious Diseases, Yale School of Medicine, New Haven, CT, USA

[7]Department of Obstetrics, Gynecology, and Reproductive Sciences, Yale School of Medicine, New Haven, CT, USA

[8] Department of Neurology, Yale School of Medicine, New Haven, CT, USA

[9] Department of Epidemiology and Microbial Diseases, Yale School of Public Health, New Haven, CT, USA

[10] Department of Pathology, Yale School of Medicine, New Haven, CT, USA

[11] Interdepartmental Program in Computational Biology and Bioinformatics, Yale University, New Haven, CT, USA

[12] Department of Molecular, Cellular, and Developmental Biology, Yale School of Medicine, New Haven, CT, USA

[13] Howard Hughes Medical Institute, Chevy Chase, MD, USA

*Corresponding authors

Corresponding authors:
Shelli F. Farhadian
135 College St.
New Haven, CT 06510
shelli.farhadian@yale.edu

Eric Song
300 Cedar St.
New Haven, CT 06510
eric.song@yale.edu

Abstract

A subset of patients with COVID-19 display neurologic symptoms but it remains unknown whether SARS-CoV-2 damages the central nervous system (CNS) directly through neuroinvasion, or if neurological symptoms are due to secondary mechanisms, including immune-mediated effects. Here, we examined the immune milieu in the CNS through the analysis of cerebrospinal fluid (CSF) and in circulation through analysis of peripheral blood mononuclear cells (PBMCs) of COVID-19 patients with neurological symptoms. Single cell sequencing with paired repertoire sequencing of PBMCs and CSF cells show evidence for unique immune response to SARS-CoV-2 in the CNS. Strikingly, anti-SARS-CoV-2 antibodies are present in the CSF of all patients studied, but the antibody epitope specificity in the CSF and relative prevalence of B cell receptor sequences markedly differed when compared to those found in paired serum. Finally, using a mouse model of SARS-CoV-2 infection, we demonstrate that localized CNS immune responses occur following viral neuroinvasion, and that the CSF is a faithful surrogate for responses occurring uniquely in the CNS. These results illuminate CNS compartment-specific immune responses to SARS-CoV-2, forming the basis for informed treatment of neurological symptoms associated with COVID-19.

Main Text

Although the primary organ dysfunction caused by SARS-CoV-2 infection is thought to be respiratory, there is growing evidence demonstrating SARS-CoV-2 effects on other major organ systems, including the central nervous system (CNS). During the current COVID-19 pandemic, case series have demonstrated neurological complications in a subset of patients[1-4]. However, the role of compartmentalized immune-mediated damage in the CNS remains incompletely understood. We examined inflammatory changes in the central nervous system (CNS) during SARS-CoV-2 infection through paired analyses of cerebrospinal fluid (CSF) and blood in patients with acute COVID-19 complicated by neurological symptoms.

Results

We enrolled hospitalized COVID-19 patients with neurological symptoms who were undergoing clinical lumbar puncture to aid in evaluation of their symptoms and consented to the collection of additional CSF for research studies. Age and sex matched SARS-CoV-2 negative community-dwelling adults were enrolled as controls (Supplementary table 1). CSF and blood samples were processed into cells from the CSF, CSF supernatant, peripheral blood mononuclear cells (PBMCs) and plasma (Fig 1a).

The divergent immunological landscape of COVID-19 patients' CSF and PBMC

Analysis of cytokines and chemokines by an ELISA-based assay showed increased inflammatory cytokines in the CSF and plasma of COVID-19 patients when compared to those of control patients, including cytokines and chemokines which have been previously observed in cytokine storm (e.g., CCL2, CXCL9, IL-8, IL-1b and IL-12). We found that the localization of specific cytokine enrichment was unique to the distinct compartments (Fig 1b and c). While CCL2, CXCL9 and IL-8 were significantly increased in the systemic circulation (plasma) of COVID-19 patients with neurological symptoms, we did not observe the same differences in the CSF (Fig 1b). Conversely, IL-1b, IL-12 and FGF-2 were elevated in the CSF of COVID-19 patients, while not in the plasma of the same patients (Fig 1c). These data indicate that, while inflammatory responses occur in both the systemic circulation and in the CNS, there are divergent responses in the two compartments, with a distinct effect of COVID-19 in the CNS on cytokines important for innate immunity and for the induction of cell-mediated immunity, including IL-12.

Next, we examined the transcriptome of cell populations in the CSF and blood using 10x single cell RNA sequencing. Our analysis included 76,473 cells from CSF and blood. We found distinct T cell, B cell and myeloid cell populations with certain subsets, such as B cells and neutrophils, enriched in the PBMC compartment compared to the CSF, which is to be expected (Figure 1d and sFig 1a-c). Since the cytokine and chemokine changes suggest an effect in the innate immune cell response to COVID-19 in the CNS, we first focused on changes occurring in these subsets. We found that COVID-19 associated transcriptional changes within innate immune cell types differed in the two compartments. While CD16+ and CD14+ monocytes included the most differentially downregulated genes in the PBMC of COVID-19 patients (Fig 1e, top two panels), dendritic cells and macrophage 2 populations included primarily differentially expressed genes in the CSF compartment (Fig 1e, middle two panels). While both CSF and peripheral macrophage 1 and NK cells showed comparable changes in the number of differentially expressed genes in COVID-19 patients, the genes affected were mostly unique to each compartment (Fig 1e, bottom two panels, sFig 1d). These data indicate compartment specific effects on innate immune cell gene transcription during this systemic viral infection.

Since we found that IL-12 is elevated in the CSF of COVID-19 patient, we analyzed the single cell transcriptomes to identify the cellular source of IL-12 in these patients, and found that the innate immune cells with the highest *IL12A* transcript expressions were the macrophage 2,

NK and dendritic cells (Fig 1f); these were also cells with large transcriptional changes in the CSF of patients when compared to controls (Fig 1e). IL-12 is thought to be produced by activated antigen presenting cells to orchestrate Th1 responses through T and NK cell activation. Consistent with this, we found evidence for activation of dendritic cells in the CSF of COVID-19 patients: 57% and 47% of the upregulated genes in these cells were classified as type 1 and type 2 interferon stimulated genes, respectively (Figure 1g). NK cells in the CSF of COVID-19 patients also specifically upregulated genes pertaining to activation states (Figure 1h). Using signaling network analysis[5,6] we find that in the CSF, these activated innate immune cell populations are predicted to interact with CD8 and CD4 T cells, suggesting a coordinated anti-viral immunological response occurring in the CSF of COVID-19 patients (Figure 1i). We asked whether the predicted interactions between activated innate and adaptive immune cells in the CNS aligned with the transcriptional change observed in the CSF T cells of COVID-19 patients. Using NicheNet, we designated the CSF innate immune cells as “sender” cells and CD4 T cells, CD8 T cells and B cells as “receiver” cells, and found enrichment in CD4 and CD8 T cells of potential regulatory genes affecting chemokine receptors, integrins and activation of immune cells, consistent with results from signaling network analysis (sFig 2).

Unique transcriptional and repertoire states of T cells exist in CSF and PBMC of COVID-19 patients.

To investigate the effects of the innate-adaptive cross talk suggested by our analysis, we first subsetted T cells found in COVID-19 patients and re-clustered them to define T cell subtypes (Figure 2a, sFig 3a-c). We found that CSF T cell populations were generally conserved in COVID-19 patients compared to controls, while among the PBMCs, there was a relative decrease in the frequency of naïve CD4 and CD8 T cell populations and increases in effector CD4 and CD8 T cells (Figure 2b). We also found significant COVID-19 associated transcriptional changes in CSF T cells (Figure 2c). This was globally true for both CD4 and CD8 T cells, and agnostic to the effector state of the cells. These transcriptional changes predicted new or dampened interactions in the CNS compartment of COVID-19 patients (sFig 4a-b) including increased T cell co-stimulation and trafficking interactions, paralleling the general immune activation in the CSF. These results demonstrate that changes in T cell subset frequency and transcriptional state occur simultaneously in the CSF and PBMC, with divergent immunological responses occurring in the CNS compartment of COVID-19 patients.

To better characterize the exchange of immune cells between the periphery and the CNS, we undertook single cell repertoire analysis to test if immune cells in the CNS undergo

local, antigen-driven selection and activation during SARS-CoV-2 infection. During neuroinflammatory conditions, CSF T and B cells resemble those in the brain parenchyma[7,8] but also develop characteristics of their circulating counterparts. If the immune response occurring in the CNS is due to a single coordinated response originating in the peripheral blood, we would expect the CSF repertoire to mirror that of the blood. As suspected, we saw T cell clones that were prevalent in the CSF were expanded in matching PBMC (Figure 2d-i). Interestingly, however, we also identified clones that were abundant in CSF but rare in the PBMC (Figure 2d-iii), and *vice versa* (Figure 2d-ii). In some cases, clones that were highly represented in the CSF (e.g. clone 5) were not found at all in the PBMC (Figure 2d-iv). Of note, we saw that the top expanded T cell clones in CSF were characterized by transcriptional profiles of Th1-like CD4 T cells and effector CD8 T cells (Figure 2a and 2d), known to be activated and expanded during a viral infection such as SARS-CoV-2.

To further dissect the dynamics of T cell expansions in the CNS, we assigned T cells as either unique or shared based on whether their TCRB V(D)Js were exclusive to one compartment or shared between compartments. Although few differences were found when comparing the diversity of mobile T cell repertoires in CSF versus PBMC, there was greater diversity of the unique T cell repertoire in the CSF of COVID-19 patients when compared to the unique T cells in the PBMC (Figure 2e). To identify the source of this difference, we examined CD4 and CD8 T cell repertoires separately. The higher diversity of unique T cells in CSF could largely be attributed to an increase in the diversity of CD8 T cells in the CSF (Figure 2i). This may reflect activation and expansion of bystander CD8 T cells in the setting of viral infection. In contrast, we observed clonal expansion of unique but not shared CD4 T cell clones in the CSF of COVID-19 patients (Figure 2f), suggesting a compartmentalized T cell response to CNS antigen.

Effector CD4 T cells in the CSF of COVID-19 patients showed unique transcriptional changes compared to CD4 T cells in the PBMC of these patients (Figure 2g). Genes that were upregulated in both Th1 and Th2 CD4 T cells from the CSF were enriched for several gene pathways important for T cell activation, along with engagement of IL-1 and IL-12 mediated signaling pathways, consistent with our observed enrichment of these cytokines in the CSF of COVID-19 patients (Figure 2h). Effector CD8 T cells in the CSF were similarly enriched for genes involved with canonical immune responses (Figure 2j): 1) increased motility and cell adhesion 2) differentiation/proliferation and 3) effector programming (responses to IL-12, IL-1, IFN-g, and T cell costimulation), indicating the presence of a coordinated T cell based immune response in the CNS (Figure 2k). Taken together, single cell analysis of T cells in COVID-19

patient CSF and PBMC reveals divergent cellular behaviors in T cells localized to the CNS and systemic circulation, with the CNS displaying increased levels of IL-12 and IL-12-associated innate and adaptive immune cell activation, diversity of effector CD8 T cells, and an expansion of CD4 T cell clones that are unique to the CSF. These data suggest the possible presence of local antigen in the CNS, and highlight the body's ability to invoke unique immune responses in each compartment.

CNS B cell responses diverge from systemic B cell responses

B cell responses are required in addition to T cell responses to develop long-lasting protective immunity to viral pathogens. We found a significant enrichment of B cells in the CSF of COVID-19 patients compared to controls (Figure 3a). Single cell RNA sequencing revealed several subtypes of B cells in the PBMC and CSF (Figure 3b, sFig 5a-c), including distinct plasma cell clusters. When the patient with the largest number of BCRs in the CSF was examined, a top expanded B cell clone was found in both the periphery and CSF. This clone comprised ~25% and ~10% of the total B cells in the two compartments, respectively. Strikingly, the top clones in each compartment had highly distinct CDR3 amino acid sequences, indicating that the primary B cell expansion in the CNS was unique to that compartment (Figure 3c). Ranking the BCR frequency in CSF and PBMC, we observed that only three clones were ranked among the top 10 clones in both compartments, and most of the shared clones were low-frequency clones in either compartment (Figure 3d), demonstrating a divergent B cell response in the CNS during COVID-19.

Next, we set out to evaluate the possible implications of the presence of divergent BCRs in the two compartments. Using a recently developed SARS-CoV-2 epitope Luminex panel[9], we found that COVID-19 patients developed antibodies specific to different regions of the spike and nucleocapsid in both the serum and CSF. However, while epitopes such as the RBD domain were broadly targeted in both compartments, we found that the region of the Spike protein 552-589 was an elevated target specific to the CSF, and the peptide mapping to Spike position 818-855 was an elevated target in the plasma and not the CSF (Figure 3e). In addition, we found that in all five patients, both the relative prevalence (rank score: 12 being most frequent, 1 being least frequent; sFig 5d, top row) and levels of antibody (sFig 5d, bottom row) diverged greatly between the CSF and plasma. Looking at the difference in rank revealed the highly heterogenous antibody response between the CSF and plasma of COVID-19 patients (Figure 3f). Thus, the anti-spike antibody and B cell repertoire sequencing demonstrated a similar

phenomenon as the T cell data; the occurrence of a generalized anti-viral, anti-SARS-CoV-2 response, but with unique features within specific compartments.

A mouse model of CNS SARS-CoV-2 infection demonstrates a compartmentalized CNS antibody response.

Neuroinvasive pathogens typically associate with intrathecal antibodies[10-12] , but it remains unknown whether antibodies in the CNS are produced locally in response to local antigen (i.e., as a consequence of neuroinvasion) or whether they reflect passive transfer of antibody from systemic circulation. This has been especially difficult to study experimentally due to the multi-organ tropism of many viral pathogens. We tested whether viral invasion into the CNS may lead to a compartmentalized antibody response using a mouse model we recently developed that reliably dissociates pulmonary and neurological infection of SARS-CoV-2[13]. By using adeno-associated virus induced expression of the human ACE2 receptor in specific tissue(s), we infected SARS-CoV-2 specifically into the lung, the brain, or both the lung and the brain (Figure 4a. sFig 6a-b). When SARS-CoV-2 infection was localized to the lung, we observed increased antibody responses in the lung and serum of mice, while we saw little antibody signal in the brain or CSF of mice (Figure 4b, red). When hACE2 was expressed in both the brain and lung and SARS-CoV-2 was administered intranasally, we saw increased antibodies in all four compartments: lung, serum, brain and CSF (Figure 4b, orange). Finally, when hACE2 was expressed in only the brain and SARS-CoV-2 was administered intracranially (producing infection in the brain but not the lung), we saw increases in antibodies in the brain and CSF, but not in the lung and serum of the mice (Figure 4b, green). These data demonstrate experimentally that CSF is a better surrogate than serum for detecting the response to SARS-CoV-2 infection of the brain, and that antibody responses in the CNS compartment can occur separately and in the absence of systemic infection.

Discussion

COVID-19 patients suffer from multi-organ dysfunction, yet the drivers of these diverse symptoms remain unclear. One possibility is that respiratory tract infection leads to a systemic cytokine storm affecting a multitude of compartments indirectly; alternatively or in addition, SARS-CoV-2 may directly invade multiple organ systems, as demonstrated by recent autopsy studies[14,15]. This latter possibility raises the question of whether each compartment has unique immunological responses to SARS-CoV-2 infection. CSF, while not identical to brain, is produced within the brain in the choroid plexus, bathes the organ, and is the only CNS tissue

surrogate readily sampled in living humans. CSF cell analyses have shed light on immune mechanisms of neuronal injury during other infections, including HIV, neurosyphilis[16], and neuroborreliosis. By assessing CSF and blood in patients with acute COVID-19 and neurological symptoms, we find evidence for a compartmentalized CNS immune response to SARS-CoV-2. We find an increase in CSF but not plasma IL-12 and IL-1b, cytokines central for coordinating innate and adaptive immune responses to invading pathogens, and further find transcriptional evidence for the role of IL-12 and IL-1 in contributing to the CNS immune response to SARS-CoV-2, with transcriptional changes in CSF effector T cells being enriched for responses to IL-12 and IL-1.

In addition to transcriptional changes found in CSF cells in COVID-19 patients, we also note unique patterns arising in the T and B cell repertoires of CSF cells. We found that CD4 T cell clones that are found only in CSF and not in the periphery are significantly expanded during COVID-19. Moreover, to our surprise, we found that although there exists some overlap between the top T cell and B cell clones found in the circulation and the CSF, by and large, the most abundant T and B cell clones were unique to each compartment.

Our data demonstrate indirect evidence for neuro-invasion of SARS-CoV-2 through the presence of antibodies produced in the CNS during SARS-CoV-2 infection. These antibodies are unique from antibodies present in serum. Using an animal model, we find that SARS-CoV-2 infection in the CNS associates with the presence of CSF antibody, and the absence of viral infection in the CNS associates with little to no antibody in CSF. The presence of anti-SARS-CoV-2 antibody in the CSF of COVID-19 patients, then, strongly suggests viral infection of the CNS.

The origins of immune responses in the CNS are still being uncovered. Although in some instances systemic responses bypass the CNS barriers after inflammation[17], it is possible that a CNS-centric circuit may invoke a local immune response[18,19]. Recent efforts have shed light on how isolated structures, such as lymph nodes, or specific regions of the gut, provide unique immunological microenvironments[20-24]; and although we know much more about metabolic and tolerogenic environments that determine immune outcomes, little is known about how the CNS compartment responds to systemic infection. We show that multiple coordinated responses, unique to each compartment, occur simultaneously during a systemic disease process. Altogether, our results suggest that neurological symptoms during COVID-19 may be due in part to a divergent immune response within the CNS, and that holistic treatment of COVID-19 may require therapies that target compartmentalized immune responses.

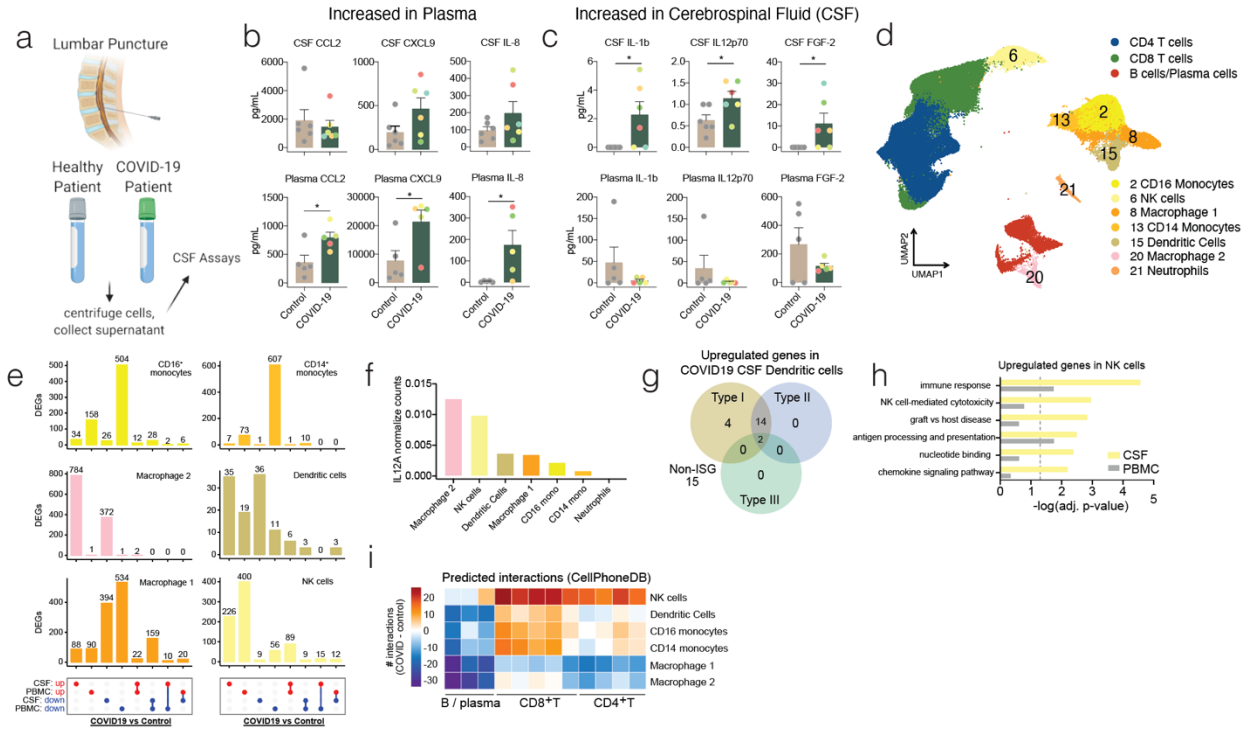

Fig. 1: Distinct immunological landscape of COVID-19 patient's CSF versus PBMC. (**a**) Schematic of study design. CSF and blood was collected from healthy and COVID-19 patients and cells were collected along with the CSF supernatant and plasma for downstream analysis. (**b** and **c**) Luminex based cytokine profiling of CSF (Top row) and plasma (Bottom row) of control and COVID-19 patients. **b,** cytokines significantly increased in plasma of COVID-19 patients but not in the CSF. **c**, cytokines significantly increased in CSF of COVID-19 patients but not in the plasma. Color of dots indicate unique patient identity(**d**) UMAP projection of 10x single cell RNA-sequencing of CSF and PBMC of healthy and COVID-19 patients. (**e**) UpSet plot showing differentially expressed genes (DEGs) in innate immune cells of COVID-19 patients versus healthy patients in CSF and PBMC. (**f**) Normalized counts of IL12A transcripts on a population level for innate immune cells. (**g**) Interferome analysis of upregulated differentially expressed genes in dendritic cells of COVID-19 patient CSF compared to healthy patient CSF. (**h**) Gene ontology enrichment of genes upregulated in NK cells of COVID-19 patients in both the CSF and PBMC. (**i**) CellPhoneDB analysis of interaction between innate immune cells and adaptive immune cells by clustering shown in Fig 1d. Number of interactions between the cells in the CSF of COVID-19 patients were subtracted by the number of interactions in the CSF of control patients to derive the heatmap. Cytokine data is derived from n = 6 for control and COVID-19 CSF, and n = 5 for control and COVID-19 plasma. Single cell RNA-seq is derived from a total of 16 libraries generated by us, and 8 additional controls from a previously published data set (n = 3 for control CSF and PBMC, n = 5 for COVID-19 CSF and PBMC, and n = 8 from Gate et al 2020). Two-tailed unpaired t-test was performed (*, P<0.05).

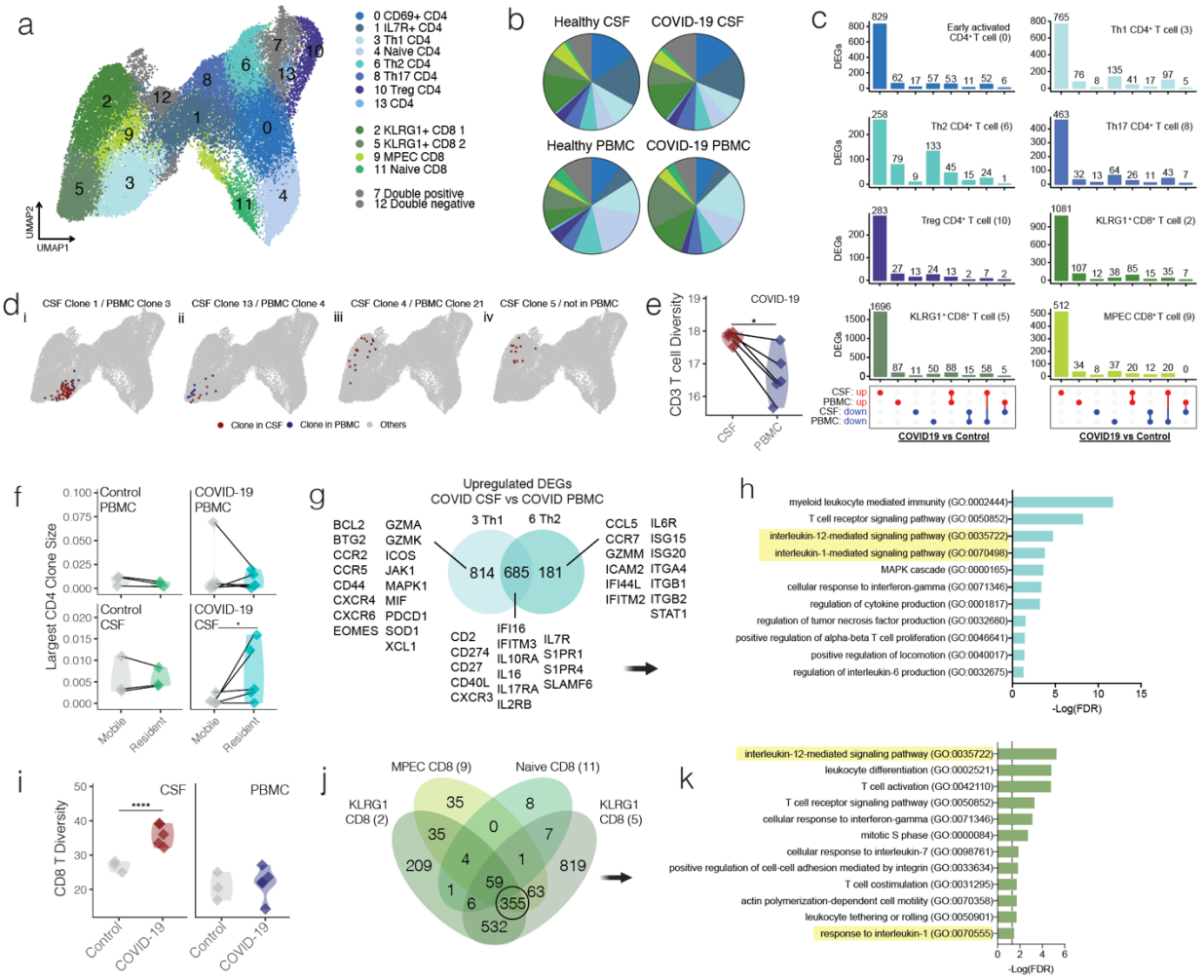

Fig 2: Transcriptional and repertoire characterization of T cells in CSF and PBMC of COVID-19 patients. (**a**) Reclustered UMAP projection of CD3+ T cells. (**b**) Pie charts depicting relative population frequency of different T cell subtypes found in CSF and PBMC of control and COVID-19 patients. (**c**) UpSet plot showing differentially expressed genes in T cells of COVID-19 patients versus healthy patients in CSF and PBMC. (**d**) Clonal T cell projection onto UMAP. Clone number denotes ranking of the clone's frequency in each compartment. i-iv. Examples of clones that are high in frequency in both CSF and PBMC (i), high in PBMC but lower in CSF (ii), high in CSF but lower in PBMC (iii), and high in CSF but not found in PBMC (iv). (**e**) Simpson diversity index of T cell repertoire found uniquely in CSF or PBMC. (**f**) The size of the most frequent CD4 T cell clone found in each compartment. (**g**) Venn diagram depicting genes upregulated in CSF of COVID-19 patients compared to PBMC of COVID-19 patients in Th1 and Th2 CD 4 T cells. (**h**) Gene ontology analysis of genes shared between Th1 and Th2 cells in Fig 2H**.** (**i**) Simpson diversity index of T cell repertoire found in CD8 T cells. (**j**) Quad-Venn diagram of genes upregulated in CSF of COVID-19 patients compared to CSF of control patients in CD8 T cells. (**k**) Gene ontology analysis of genes shared between the three effector CD8 T cell subtypes in Fig 2j. one-tailed paired t-test was performed (*, P<0.05; ****, P<0.0001).

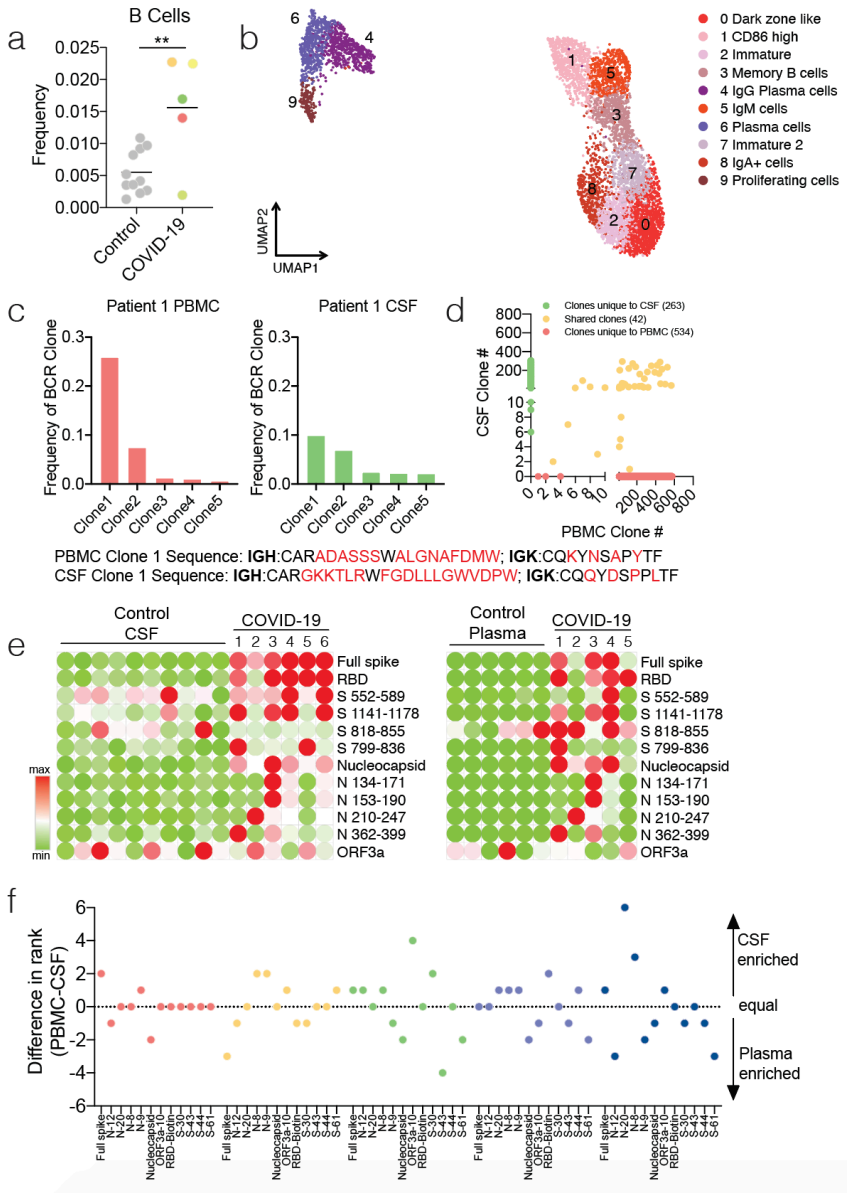

Fig 3: Central nervous system localized B cell responses occur in COVID-19 patients. (**a**) Frequency of B cells found in CSF of control and COVID-19 patients. (**b**) Reclustered UMAP projection of cells with BCRs. (**c**) Bar graph depicting frequency of top five most expanded clones in PBMC and CSF of a patient. Bottom text shows uniquely distinct sequences in the top clones of this patient (shown in red). (**d**) Graph depicting overlap of clones found in CSF and PBMC of a patient. Green depicts clones only found in CSF, orange clones shared between the CSF and PBMC, and red, clones unique to PBMC. Yellow box depicts clones that would fall under top 10 most frequent clones in each compartment (lower clone rank # describes more frequent clone). (**e**) Luminex based assay showing binding of epitopes of SARS-CoV-2 from antibodies found in CSF (left) and plasma (right) of control and COVID-19 patients. (**f**) Epitope frequency was ranked in each patient sample individually, and a difference in rank number for each cluster was graphed to determine CSF (positive) or Plasma (negative) enriched antibody epitopes. Two-tailed unpaired t-test was performed (**, P<0.01).

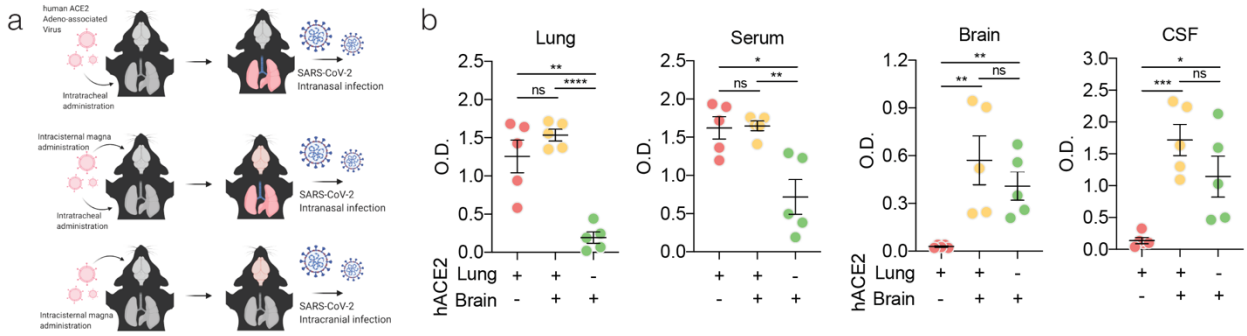

Figure 4: Cerebrospinal fluid antibodies reflect localized central nervous system infection. (**a**) Schematic of experimental procedure for (**b**). Mice were given localized AAV-hACE2 to overexpress human ACE2 in either the lung (top), brain and lung (middle) or brain only (bottom). After two weeks, mice were infected with SARS-CoV-2. (**b**) ELISA against SARS-CoV-2 spike protein was performed with lung homogenates, serum, brain homogenates and CSF. n = 5 for all three conditions. Two-tailed unpaired t-test was performed (*, P<0.05; **, P<0.01; ***, P<0.005; ****, P<0.0001).

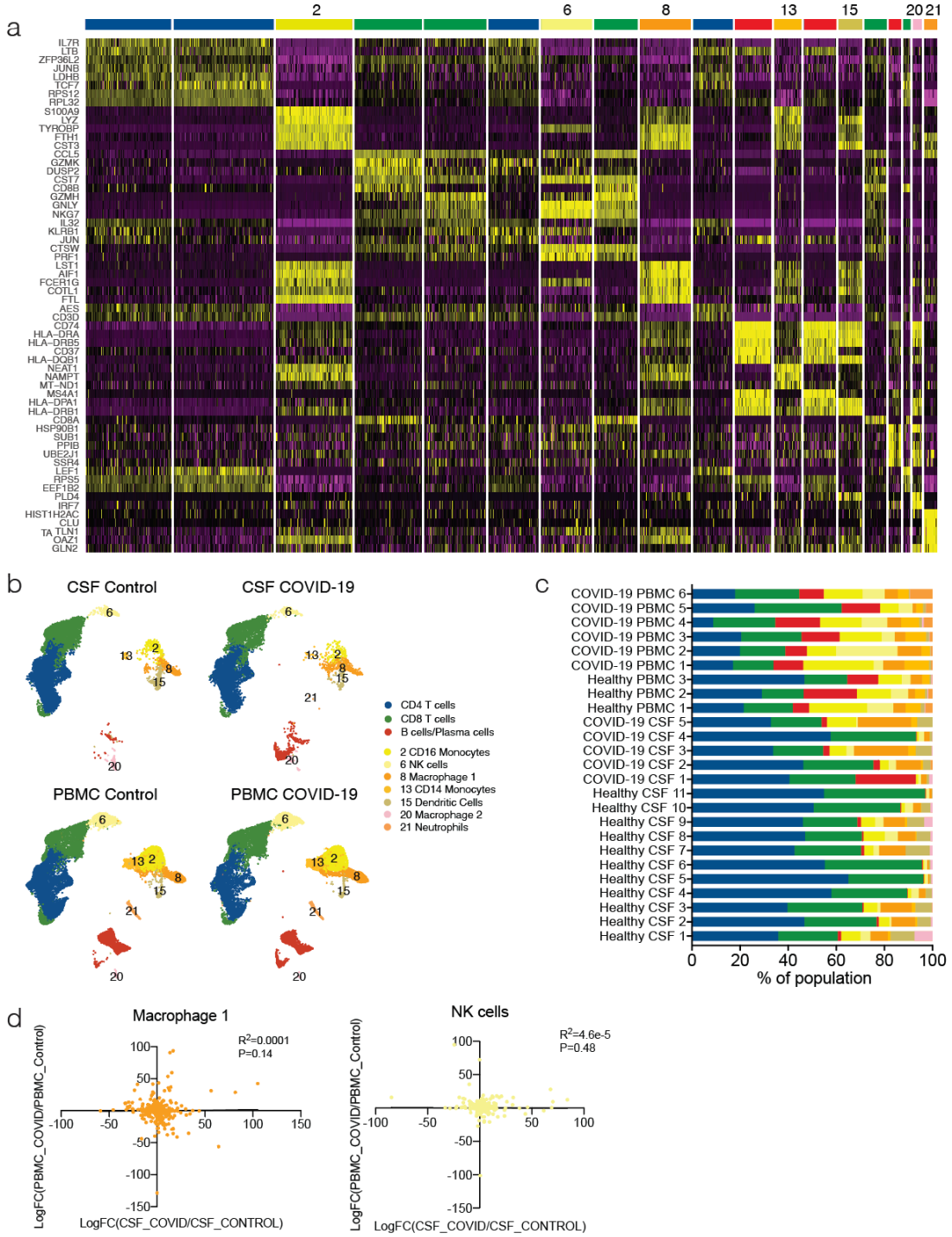

Fig. s1 Distinct immunological landscape of COVID-19 patient's CSF versus PBMC. (**a**) Top DEGs distinguishing clusters found in Figure 1. (**b**) UMAP projection of cell types in CSF and PBMC of COVID-19 patients and control patients. (**c**) Relative proportion of cell types found in biological samples for the study. (**d**) Correlation of Log fold change of genes in COVID-19 patient CSF versus PBMC in macrophages and NK cells.

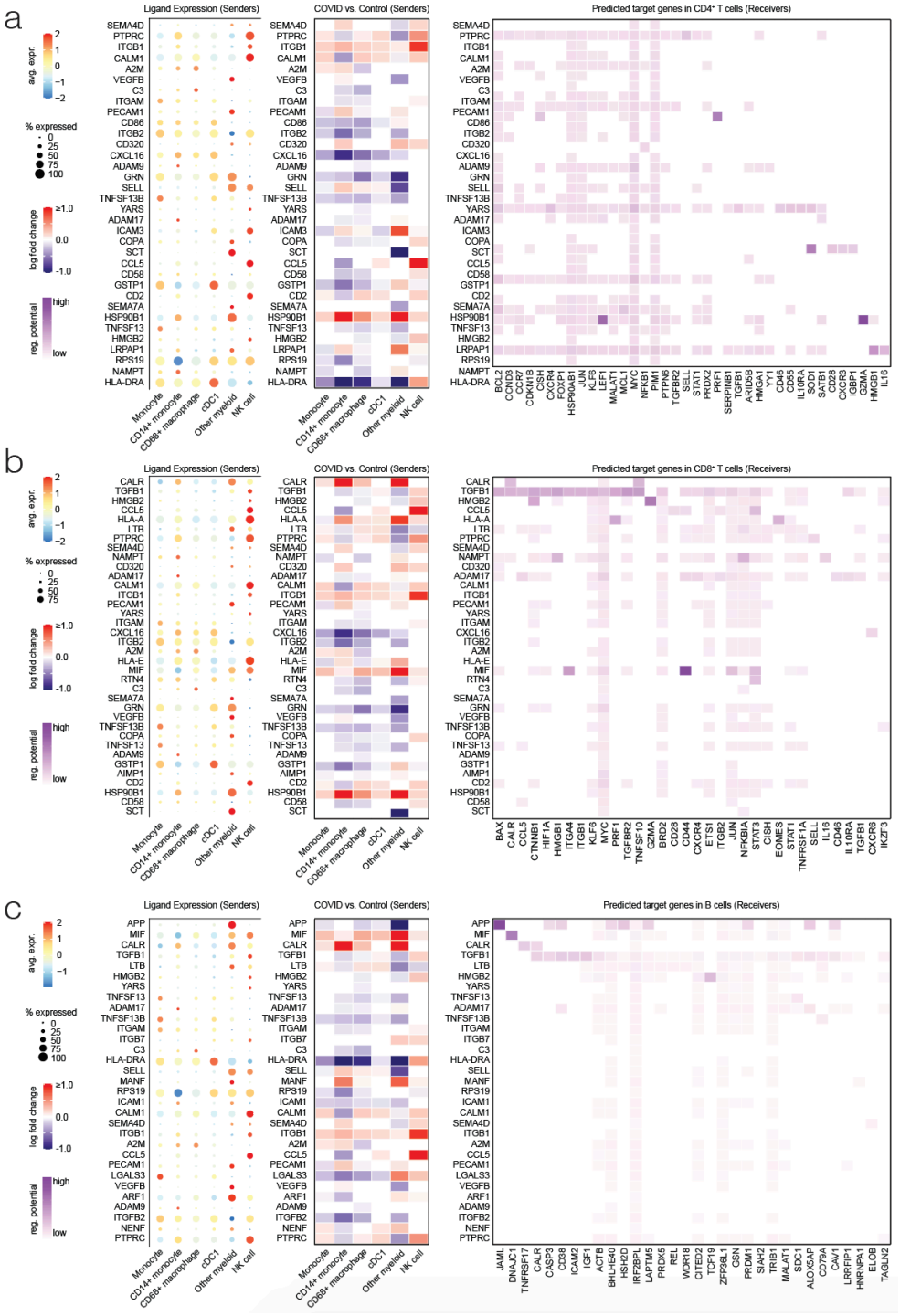

Fig. s2: Interaction of innate and adaptive immune cells predicted by NicheNet. NicheNet analysis of innate immune cell interaction with CD8 T cells. Left panel shows relative expression levels of ligands expressed in different innate immune cell compartments. Middle panel shows the change in each ligand in COVID-19 patient CSF versus control patient CSF. Right panel shows a heatmap of probability of regulatory potential of these ligands (y-axis) to affect the differentially expressed genes in the receiver. (**a**) Shows analysis with receivers as CD4 T cells. (**b**) Shows analysis with receivers as CD8 T cells. (**c**) Shows analysis with receivers as B cells.

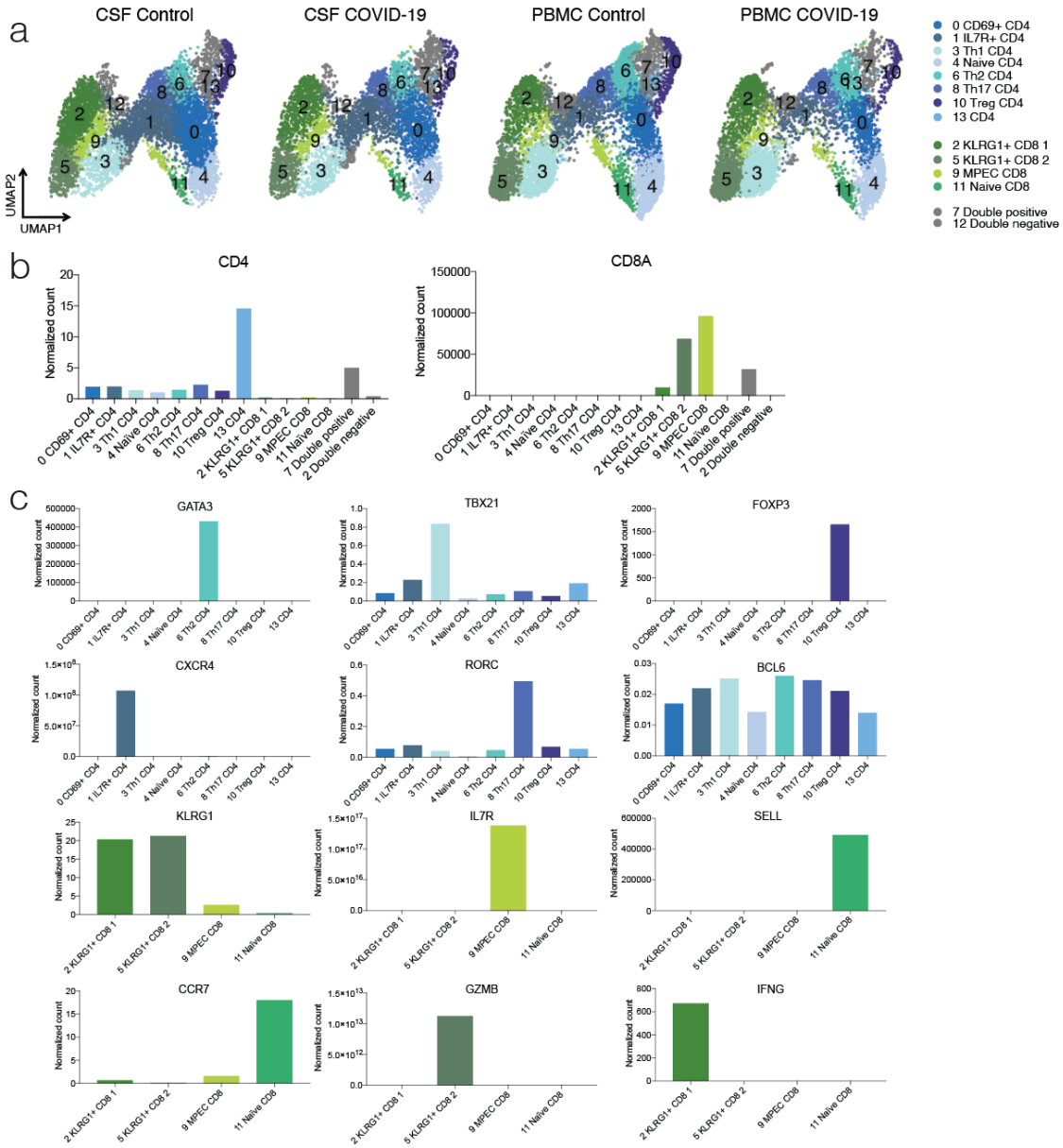

Fig. s3 Characterization of T cell subsets found in CSF and PBMC. (**a**) UMAP projection of T cell types in CSF and PBMC of COVID-19 patients and control patients. (**b**) Normalized gene expression data of T cell identification genes in T cells

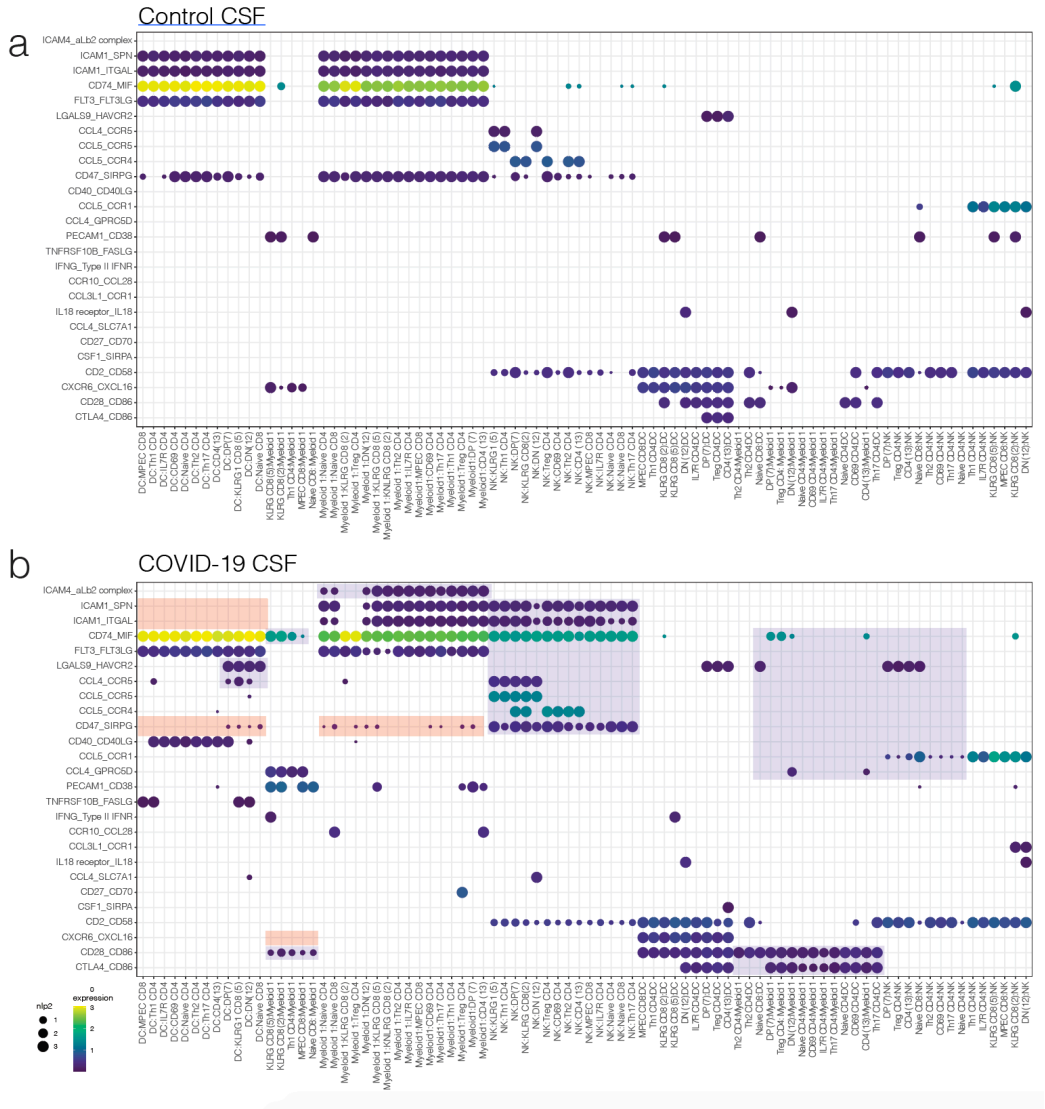

Fig. s4: Predicted interaction enriched in CSF of COVID-19 patients using CellPhoneDB CellPhoneDB interaction map between innate immune cells identified in Fig 1D and T cell subtypes identified in Fig 2A of COVID-19 patient CSF. (**a**) Depicts control patient CSF interactions. (**b**) Depicts interactions in CSF of COVID-19 patients. Red box depicts interactions disappearing compared to control CSF and blue box depicts interactions enriched compared to control CSF.

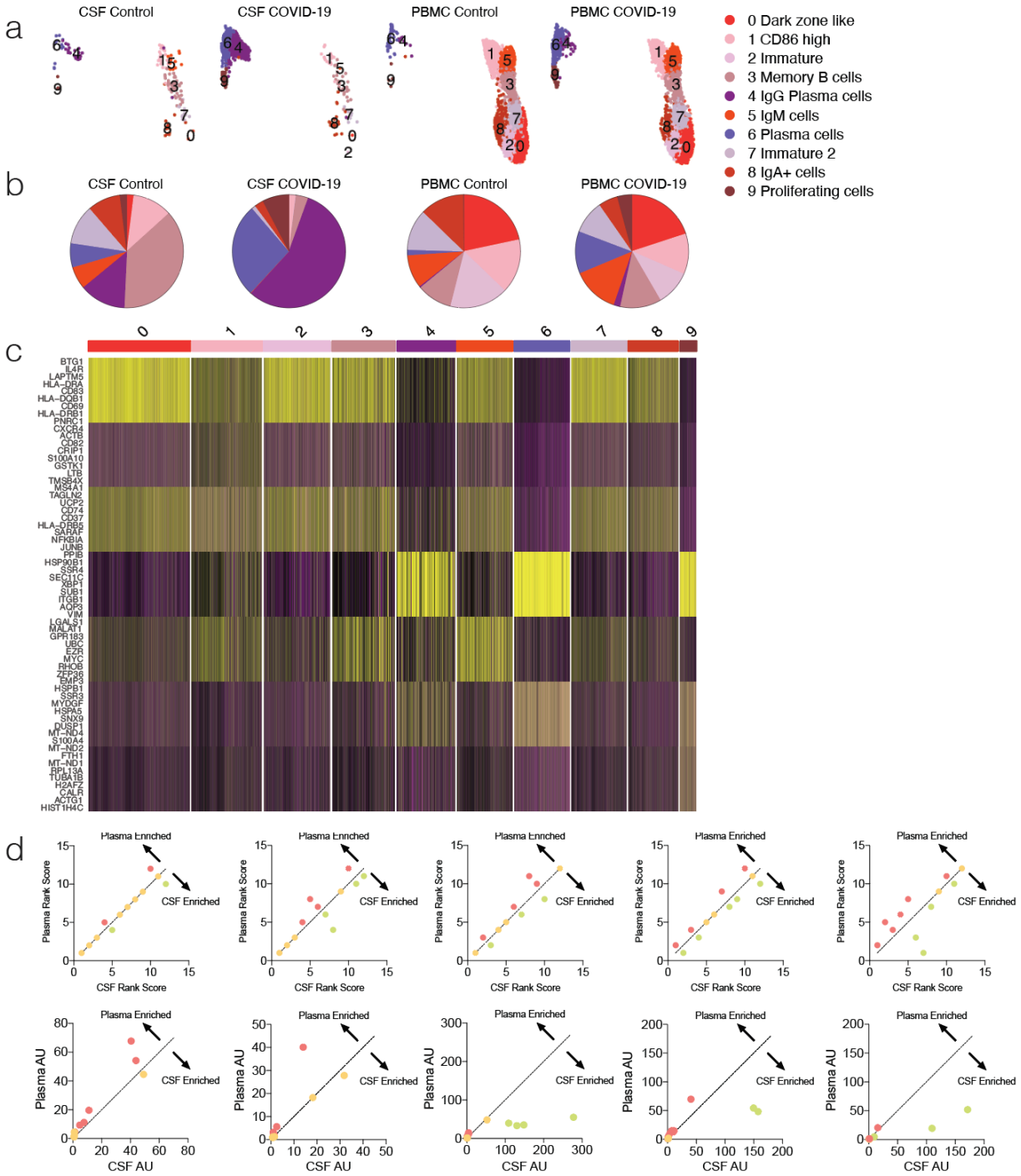

Fig s5: CNS localized B cell responses occur in COVID-19 patients.
(**a**) UMAP projection of B cell types in CSF and PBMC of COVID-19 patients and control patients. (**b**) Pie charts depicting relative population frequency of different B cell subtypes found in CSF and PBMC of control and COVID-19 patients. (**c**) Top DEGs distinguishing clusters found in Figure 3. (**d, top row**) SARS-CoV-2 epitope binding antibody frequency from e was ranked and correlation between CSF and plasma was performed (higher rank score depicts more frequent epitope. (**d, bottom row**). Similar to top row, but normalized arbitrary unit was used to derive a correlation between plasma and CSF antibodies.

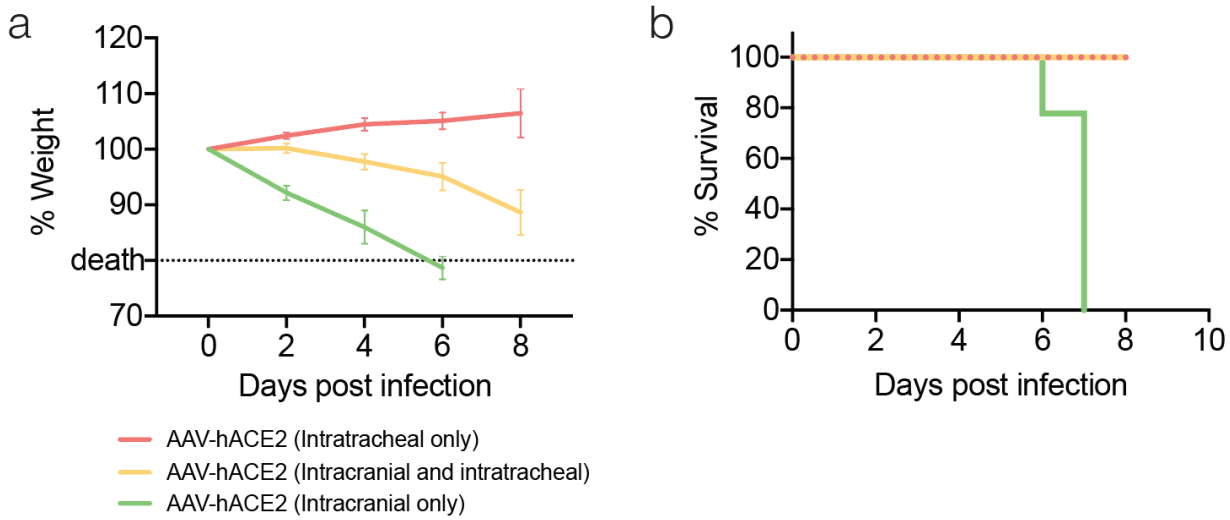

Fig s6: CNS localized B cell responses occur in COVID-19 patients.
Refer to Figure 4 for experiment design. (**a**) Weight loss curve for mice described in Figure 4. (**b**) Kaplan meier curve of mice described in Figure 4 (death was determined by weight loss).

Participant#	***1***	***2***	***3***	***4***	***5***	***6***
Age	43	84	60	67	55	64
ICU Status	ICU	Non-ICU	ICU	ICU	Non-ICU	ICU
Mechanical Ventilation	No	No	Yes	Yes	No	Yes
Neurological Symptoms	Encephalopathy	Intractable headache, Encephalopathy	Seizures	Encephalopathy, neuromuscular weakness	Intractable headache and blurred vision	Encephalopathy
CSF						
White blood Cells (cells/uL)	3	2	2	0	1	0
Protein (mg/dL)	57.4	29.3	66	85.6	20.5	48.3

Supplementary Table 1. Clinical characteristic of patients.

Supplementary Table 2. Normalized gene counts for clusters in Figure 1.

Supplementary Table 3. Differentially expressed genes in clusters described in Figure 1 between (a) COVID-19 patient CSF versus Control patient CSF. (**b**) COVID-19 patient PBMC versus Control patient PBMC. (**c**) COVID-19 patient CSF versus COVID-19 patient PBMC

Supplementary Table 4. Normalized gene counts for T cell clusters in Figure 2.

Supplementary Table 5. Differentially expressed genes between genes in T cell clusters described in Figure 2 (a) COVID-19 patient CSF versus Control patient CSF. (**b**) COVID-19 patient PBMC versus Control patient PBMC. (**c**) COVID-19 patient CSF versus COVID-19 patient PBMC

Supplementary Table 6. Normalized gene counts for B cell clusters in Figure 3.

Methods:

Study participants. COVID-19 patients admitted to Yale New Haven Hospital (YNHH) in March-May 2020 were recruited to the IRB approved Yale IMPACT study (Implementing Medical and Public Health Action Against Coronavirus CT). Patients who were positive for SARS-CoV-2 by nasopharyngeal swab RT-PCR and who were undergoing clinical lumbar puncture for evaluation of neurological symptoms were included. Negative controls were recruited from the surrounding community, and were confirmed to be negative for SARS-CoV-2 infection by PCR. All participants or their designated surrogate consented to donate 25cc of CSF for research studies. Blood was collected within one hour of lumbar puncture.

Tissue collection. CSF was centrifugfed at 400G for 8 minutes, with cell-free supernatant removed for cytokine and antibody assays, and cell pellet processed for single cell RNA sequencing, as below. PBMCs were isolated from blood by layering diluted blood (1:1 in PBS) on top of an equal volume of Ficoll, followed by centrifugation and isolation of the buffy coat. CSF and blood cells were processed immediately for single cell RNA sequencing. CSF supernatant and plasma were stored at -80 for less than two months before cytokine and antibody analysis.

Cytokine assays. Soluble chemokines and cytokines were assessed in CSF supernatant and paired plasma using the HD71 Human Cytokine Array/Chemokine Array 71-plex panel (Eve Technologies, Calgary, AB). All samples were run in duplicate and the average measurement for each analyte was used for analysis.

Single cell RNA sequencing. Approximately 8,000 single cells from CSF and from PBMC were loaded into each channel of a Chromium single-cell 5′ Chip (V3 technology). 5’ 10X libraries were sequenced on Illumina Novaseq at approximately 50,000 reads per cell. Raw seqeuncing reads were aligned to the human GRCh38 genome and gene counts were quantified as UMIs using Cell Ranger count v3.0 (10x Genomics). We removed cells with >10% mitochondrial RNA content, and included cells with > 500 and <2000 genes expressed per cell. Dimensionality reduction, clustering, and visualization was performed using Seurat, with further analyses performed using CellPhoneDB and NicheNet. For differential expression analysis, markers for each cluster were determined by comparing the cells of each cluster to all other cells using the FindMarkers function in Seurat. For all comparisons between groups and clusters, only genes expressed by at least 10% of cells were included. The R package ggplot2 (v.3.1.0) was used to

plot the results of differential expression analyses, showing the average log-transformed fold change of each gene and the −log10 of the adjusted *P* value (Benjamini–Hochberg correction). Interferon regulated genes were identified using Interferome. Differential expression analysis was performed in Seurat v3 (Stuart et al., 2019) using the two-tailed Wilcoxon test, comparing cells from COVID-19 patients vs healthy controls. Significant differentially expressed genes (DEGs) were defined as: adjusted $p < 0.05$ and |log fold change| ≥ 0.1. Gene ontology and pathway enrichment analysis was performed using DAVID (Huang et al., 2009). DEGs in PBMC and CSF samples were compared using the UpSetR package.

To identify potential intercellular interactions between different cell types in the scRNA-seq data, we utilized CellPhoneDB v2 (Efremova et al., 2020). Normalized count matrices and associated cell type labels were provided to CellPhoneDB and analyzed under both the statistical mode and the thresholding mode. Of note, since the statistical mode of CellPhoneDB seeks to assess the specificity of a given interaction, a lack of statistical significance does not necessarily mean a given interaction is not present. Therefore, when comparing the number of potential intercellular interactions in COVID-19 patients vs healthy controls, the simpler threshold-based analysis mode was used. In contrast, for pinpointing the top candidate cell-cell interactions in each dataset, the statistical analysis mode was used, with a significance threshold of $p < 0.05$.

To further explore the downstream consequences of these intercellular interactions, we performed NicheNet analysis (Browaeys et al., 2020). The cDC1, NK cell, monocyte, macrophage, and myeloid cell clusters were defined as the potential “sender” cell populations. Different lymphocyte populations were defined as potential “receiver” cells: all CD4 T cells merged across clusters, merged CD8 T cells, or merged B cells. Potential ligands and receptors were defined as being expressed in ≥ 20% of cells in a particular cell type. Differentially expressed genes (i.e. candidate target genes) were defined similarly as above, with adjusted $p < 0.05$ and |log fold change| ≥ 0.1.

TCR and BCR analysis. Single cell V(D)J sequences were generated using cellranger vdj function. Assignments of V(D)J sequences were performed using IgBLAST v.1.6.1 with the September 12, 2018 version of the IMGT gene database (as described previously[25,26]). Non-functional V(D)J sequences were removed. Cells with multiple IGH, TCRA or TCRB V(D)J sequences were assigned to the most abundant V(D)J sequence by unique molecular identifier count (and based on numbers of sequenced reads in instances with ties). B cell clones in the CSF and circulation were identified using an approach described previously using hierarchical

clustering implemented using the DefineClones.py function of Change-O v0.3.4 and a junctional sequence hamming dissimilarity threshold of 0.17[26]. To account for the presence of light chains, heavy chain-based clones were corrected for using an approach described previously[27]. T cell clones in the CSF and circulation were identified if they shared the same (IMGT-aligned) TCRB V(D)J sequence and the same TCRA V(D)J sequence. Analysis was completed using methods described previously. Abundance and diversity analysis were performed using the alphaDiversity function in Alakazam v1.0.2 with a Hill Diversity index set to 2 corresponding to Simpson's diversity; 2000 bootstrap replicates from the Chao-estimator corrected abundance distribution under rarefaction set to the depth of the smallest sample were used.

T and B cell clustering. We initially combined all 76,473 CSF and blood cells and generated clusters using Seurat. For each cluster we assigned a cell-type label using statistical enrichment for sets of marker genes, and manual evaluation of gene expression for small sets of known marker genes. We then created a separate Seurat object consisting only of T cells clusters from the original analysis, and a separate Seurat object consisting only of plasma and B cells. We then re-clustered these T and B cells and annotated sub-clusters using previously annotated marker genes.

SARS-CoV-2 Serological Assay. CSF and plasma were assessed for antibodies using ReScan (https://www.medrxiv.org/content/10.1101/2020.05.11.20092528v1), a custom phage-display library consisting of nine SARS-CoV-2 antigens.

Mice. Six to twelve-week-old mixed sex C57Bl/6 (B6J) purchased from Jackson laboratories, and B6.Cg-Tg(K18-ACE2)2Prlmn/J(K18-hACE2) mice (gift from Jackson Laboratories) were subsequently bred and housed at Yale University. All procedures used in this study (sex-matched, age-matched) complied with federal guidelines and the institutional policies of the Yale School of Medicine Animal Care and Use Committee.

AAV infection (Intratracheal and Intracisternal magna injection). Adeno-associated virus 9 encoding hACE2 were purchased from Vector biolabs (AAV-CMV-hACE2).

Intratracheal injection. Animals were anaesthetized using a mixture of ketamine (50 mg kg^{-1}) and xylazine (5 mg kg^{-1}), injected intraperitoneally. The rostral neck was shaved and disinfected. A 5mm incision was made and the salivary glands were retracted, and trachea was visualized.

Using a 500µL insulin syringe a 50µL bolus injection of 10^{11}GC of AAV-CMV-hACE2 was injected into the trachea. The incision was closed with VetBond skin glue. Following intramuscular administration of analgesic (Meloxicam and buprenorphine, 1 mg kg^{-1}), animals were placed in a heated cage until full recovery.

Intracisternal magna injection. Mice were anesthetized using ketamine and xylazine, and the dorsal neck was shaved and sterilized. A 2 cm incision was made at the base of the skull, and the dorsal neck muscles were separated using forceps. After visualization of the cisterna magna, a Hamilton syringe with a 15 degree 33 gauge needle was used to puncture the dura. 3µL of AAV_9 (3.10^{12} viral particles/mouse) or mRNA (4-5 µg) was administered per mouse at a rate of 1µL min^{-1}. Upon completion of the injection, needle was left in to prevent backflow for an additional 3 minutes. The skin was stapled, disinfected and same post-operative procedures as intratracheal injections were performed.

Generation of SARS-CoV-2 virus. To generate SARS-CoV-2 viral stocks, Huh7.5 cells were inoculated with SARS-CoV-2 isolate USA-WA1/2020 (BEI Resources #NR-52281) to generate a P1 stock. To generate a working stock, VeroE6 cells were infected at a MOI 0.01 for four days. Supernatant was clarified by centrifugation (450g x 5min) and filtered through a 0.45 micron filter. To concentrate virus, one volume of cold (4 °C) 4x PEG-it Virus Precipitation Solution (40% (w/v) PEG-8000 and 1.2M NaCl) was added to three volumes of virus-containing supernatant. The solution was mixed by inverting the tubes several times and then incubated at 4 °C overnight. The precipitated virus was harvested by centrifugation at 1,500 x g for 60 minutes at 4 °C. The pelleted virus was then resuspended in PBS then aliquoted for storage at -80°C. Virus titer was determined by plaque assay using Vero E6 cells.

SARS-CoV-2 infection (intranasal). Mice were anesthetized using 30% v/v Isoflurane diluted in propylene glycol. Using a pipette, 50µL of SARS-CoV-2 ($3x10^7$ PFU/ml) was delivered intranasally.

SARS-CoV-2 infection (intraventricular). Animals were anaesthetized using a mixture of ketamine (50 mg kg^{-1}) and xylazine (5 mg kg^{-1}), injected intraperitoneally. After sterilization of the scalp with alcohol and betadine, a midline scalp incision was made to expose the coronal and sagittal sutures, and a burr holes were drilled 1 mm lateral to the sagittal suture and 0.5 mm posterior to the bregma. A 10 µl Hamilton syringe loaded with virus, and was inserted into the burr hole at a depth of 2 mm from the surface of the brain and left to equilibrate for

1 min before infusion. Once the infusion was finished, the syringe was left in place for another minute before removal of the syringe. Bone wax was used to fill the burr hole and skin was stapled and cleaned. Following intramuscular administration of analgesic (Meloxicam and buprenorphine, 1 mg kg^{-1}), animals were placed in a heated cage until full recovery. For high condition, 5µL of SARS-CoV-2 ($3x10^7$ PFU/ml) and for low condition 5µL of SARS-CoV-2 ($3x10^6$ PFU/ml) was used.

Enzyme-linked immunosorbent assay. ELISAs were performed as previously reported [28]. In short, Triton X-100 and RNase A were added to serum samples at final concentrations of 0.5% and 0.5mg/ml respectively and incubated at room temperature (RT) for 3 hours before use to reduce risk from any potential virus in serum. 96-well MaxiSorp plates (Thermo Scientific #442404) were coated with 50 µl/well of recombinant SARS Cov-2 S1 protein (ACROBiosystems #S1N-C52H3-100ug) at a concentration of 2 µg/ml in PBS and were incubated overnight at 4 °C. The coating buffer was removed, and plates were incubated for 1h at RT with 200µl of blocking solution (PBS with 0.1% Tween-20, 3% milk powder). Serum was diluted 1:50 in dilution solution (PBS with 0.1% Tween-20, 1% milk powder) and 100µl of diluted serum was added for two hours at RT. Plates were washed three times with PBS-T (PBS with 0.1% Tween-20) and 50µl of mouse IgG-specific secondary antibody (BioLegend #405306, 1:10,000) diluted in dilution solution added to each well. After 1h of incubation at RT, plates were washed three times with PBS-T. Samples were developed with 100µl of TMB Substrate Reagent Set (BD Biosciences #555214) and the reaction was stopped after 15 min by the addition of 2 N sulfuric acid.

Statistical methods. All statistical analyses were performed using commercially available software (Prism or Excel). All values are expressed as the mean ± SEM. Differences in means between two groups were analysed using unpaired two-sided *t*-tests, unless otherwise noted. For scRNA-seq analyses, we corrected for multiple comparisons and report adjusted P values using Benjamini–Hochberg correction. For pathway analyses, Fisher's exact test was used with Bonferroni correction for multiple testing.

Schematics. Images in Figure 1, Figure 4 and Figure s6 were created with Biorender.com

Data availability

Gene expression and repertoire data in the study are available in the NCBI repository SRAxxxx

Competing Interests

None of the authors declare interests related to the manuscript.

Materials & Correspondence

Correspondence and material requests should be addressed to shelli.farhadian@yale.edu

Requests for scripts, code and raw data used in this study should be addressed to eric.song@yale.edu

Acknowledgements. This work was supported by NIH, K23MH118999 (SFF), F30CA239444 (ES), F30CA250249 (RDC), 1R01AI157488 (AI and SFF), R01AI104739 (SHK), U19AI089992 (SHK, AI), NIH T32GM136651 (ES, RDC, RJ), the Beatrice Kleinberg Neuwirth Fund (AIK), and by Fast Grant funding support from the Emergent Ventures at the Mercatus Center, George Mason University (AI). We thank James A. Wells, James R. Byrnes and Joseph L. DeRisi for their contribution of reagents to assist with the serologic assays. And we thank everyone involved in this study, especially the patients who volunteered to be a part of this study, members of the Iwasaki Lab for their insightful discussions (Patrick Wong, Orr-el Weizman), members of the Yale Impact Team (especially Nathan Grubaugh, Chantal Vogels, Tianyang Mao, Jonathan Klein, Carolina Lucas, Jieun Oh), the Yale environmental health and safety (EHS) team, and the team at Yale center for genome analysis (YCGA).

References

1 Huang, C. *et al.* Clinical features of patients infected with 2019 novel coronavirus in Wuhan, China. *Lancet* **395**, 497-506, doi:10.1016/s0140-6736(20)30183-5 (2020).

2 Netland, J., Meyerholz, D. K., Moore, S., Cassell, M. & Perlman, S. Severe acute respiratory syndrome coronavirus infection causes neuronal death in the absence of encephalitis in mice transgenic for human ACE2. *J Virol* **82**, 7264-7275, doi:10.1128/jvi.00737-08 (2008).

3 Zhang, H. Early lessons from the frontline of the 2019-nCoV outbreak. *Lancet* **395**, 687, doi:10.1016/s0140-6736(20)30356-1 (2020).

4 Kim, J. E. *et al.* Neurological Complications during Treatment of Middle East Respiratory Syndrome. *J Clin Neurol* **13**, 227-233, doi:10.3988/jcn.2017.13.3.227 (2017).

5 Efremova, M., Vento-Tormo, M., Teichmann, S. A. & Vento-Tormo, R. CellPhoneDB: inferring cell-cell communication from combined expression of multi-subunit ligand-receptor complexes. *Nat Protoc* **15**, 1484-1506, doi:10.1038/s41596-020-0292-x (2020).

6 Browaeys, R., Saelens, W. & Saeys, Y. NicheNet: modeling intercellular communication by linking ligands to target genes. *Nat Methods* **17**, 159-162, doi:10.1038/s41592-019-0667-5 (2020).

7 Lovato, L. *et al.* Related B cell clones populate the meninges and parenchyma of patients with multiple sclerosis. *Brain* **134**, 534-541, doi:10.1093/brain/awq350 (2011).

8 Salou, M. *et al.* Expanded CD8 T-cell sharing between periphery and CNS in multiple sclerosis. *Ann Clin Transl Neurol* **2**, 609-622, doi:10.1002/acn3.199 (2015).
9 Zamecnik, C. R. *et al.* ReScan, a Multiplex Diagnostic Pipeline, Pans Human Sera for SARS-CoV-2 Antigens. *medRxiv*, 2020.2005.2011.20092528, doi:10.1101/2020.05.11.20092528 (2020).
10 Marfin, A. A. & Gubler, D. J. West Nile encephalitis: an emerging disease in the United States. *Clin Infect Dis* **33**, 1713-1719, doi:10.1086/322700 (2001).
11 Djukic, M. *et al.* Cerebrospinal fluid findings in adults with acute Lyme neuroborreliosis. *J Neurol* **259**, 630-636, doi:10.1007/s00415-011-6221-8 (2012).
12 Nagel, M. A. *et al.* The value of detecting anti-VZV IgG antibody in CSF to diagnose VZV vasculopathy. *Neurology* **68**, 1069-1073, doi:10.1212/01.wnl.0000258549.13334.16 (2007).
13 Song, E. *et al.* Neuroinvasive potential of SARS-CoV-2 revealed in a human brain organoid model. *bioRxiv*, 2020.2006.2025.169946, doi:10.1101/2020.06.25.169946 (2020).
14 Puelles, V. G. *et al.* Multiorgan and Renal Tropism of SARS-CoV-2. *N Engl J Med* **383**, 590-592, doi:10.1056/NEJMc2011400 (2020).
15 Solomon, I. H. *et al.* Neuropathological Features of Covid-19. *N Engl J Med*, doi:10.1056/NEJMc2019373 (2020).
16 Marra, C. M., Maxwell, C. L., Dunaway, S. B., Sahi, S. K. & Tantalo, L. C. Cerebrospinal Fluid Treponema pallidum Particle Agglutination Assay for Neurosyphilis Diagnosis. *J Clin Microbiol* **55**, 1865-1870, doi:10.1128/JCM.00310-17 (2017).
17 Iijima, N. & Iwasaki, A. Access of protective antiviral antibody to neuronal tissues requires CD4 T-cell help. *Nature* **533**, 552-556, doi:10.1038/nature17979 (2016).
18 Louveau, A. *et al.* CNS lymphatic drainage and neuroinflammation are regulated by meningeal lymphatic vasculature. *Nat Neurosci* **21**, 1380-1391, doi:10.1038/s41593-018-0227-9 (2018).
19 Song, E. *et al.* VEGF-C-driven lymphatic drainage enables immunosurveillance of brain tumours. *Nature* **577**, 689-694, doi:10.1038/s41586-019-1912-x (2020).
20 Esterhazy, D. *et al.* Compartmentalized gut lymph node drainage dictates adaptive immune responses. *Nature* **569**, 126-130, doi:10.1038/s41586-019-1125-3 (2019).
21 Mora, J. R. *et al.* Selective imprinting of gut-homing T cells by Peyer's patch dendritic cells. *Nature* **424**, 88-93, doi:10.1038/nature01726 (2003).
22 Dudda, J. C., Simon, J. C. & Martin, S. Dendritic cell immunization route determines CD8+ T cell trafficking to inflamed skin: role for tissue microenvironment and dendritic cells in establishment of T cell-homing subsets. *J Immunol* **172**, 857-863, doi:10.4049/jimmunol.172.2.857 (2004).
23 Meng, W. *et al.* An atlas of B-cell clonal distribution in the human body. *Nat Biotechnol* **35**, 879-884, doi:10.1038/nbt.3942 (2017).
24 Stern, J. N. *et al.* B cells populating the multiple sclerosis brain mature in the draining cervical lymph nodes. *Sci Transl Med* **6**, 248ra107, doi:10.1126/scitranslmed.3008879 (2014).
25 Lefranc, M. P. *et al.* IMGT, the international ImMunoGeneTics database. *Nucleic Acids Res* **27**, 209-212, doi:10.1093/nar/27.1.209 (1999).
26 Jiang, R. *et al.* Single-cell repertoire tracing identifies rituximab-resistant B cells during myasthenia gravis relapses. *JCI Insight* **5**, doi:10.1172/jci.insight.136471 (2020).
27 Oh, J. E. *et al.* Migrant memory B cells secrete luminal antibody in the vagina. *Nature* **571**, 122-126, doi:10.1038/s41586-019-1285-1 (2019).
28 Israelow, B. *et al.* Mouse model of SARS-CoV-2 reveals inflammatory role of type I interferon signaling. *bioRxiv*, doi:10.1101/2020.05.27.118893 (2020).